Electronic Supplementary Information (ESI)

Electrochemical Behavior of a Ni_3N OER Precatalyst in Fe-Purified Alkaline Media: The Impact of Self-Oxidation and Fe Incorporation

Kenta Kawashima,[1] Raúl A. Márquez-Montes,[1] Hao Li,[1,2] Kihyun Shin,[1,2] Chi L. Cao,[3] Kobe M. Vo,[3] Yoon Jun Son,[3] Bryan R. Wygant,[1] Adithya Chunangad,[3] Duck Hyun Youn,[4] Graeme Henkelman,[1,2] Víctor H. Ramos-Sánchez,[5] C. Buddie Mullins[1,3,6,7,*]

[1]*Department of Chemistry, The University of Texas at Austin, Austin, Texas 78712, United States*

[2]*Oden Institute for Computational Engineering and Sciences, The University of Texas at Austin, Austin, Texas 78712, United States*

[3]*McKetta Department of Chemical Engineering, The University of Texas at Austin, Austin, Texas 78712, United States*

[4]*Department of Chemical Engineering, Interdisciplinary Program in Advanced Functional Materials and Devices Development, Kangwon National University, Chuncheon, Gangwon-do 24341, South Korea*

[5]*Facultad de Ciencias Químicas, Universidad Autónoma de Chihuahua, Chihuahua, Chihuahua 7 31125, México*

[6]*Center for Electrochemistry, The University of Texas at Austin, Austin, Texas 78712, United States*

[7]*H2@UT, The University of Texas at Austin, Austin, Texas 78712, United States*

**Corresponding author.*

E-mail address: mullins@che.utexas.edu

Electrolyte Purification for Standard Three-Electrode Cell Tests

Fe Adsorbent Preparation

Regent grade 1 M KOH aqueous electrolyte [prepared from KOH flakes (90%, Sigma Aldrich)] was purified by a $Ni(OH)_2$-based process, which is a slight modification of a previously reported procedure.[1] 2 g of nickel(II) nitrate hexahydrate (99%, Acros Organics) was installed in a 50 mL polypropylene centrifuge tube and completely dissolved in 4 mL of ultra-pure water (18 MΩ resistance). Subsequently, to the as-prepared aqueous solution, 20 mL of regent grade 1 M KOH was added, resulting in the formation of a $Ni(OH)_2$ precipitate (a light-green solid). After shaking, the as-obtained mixture was centrifuged at 8500 rpm for 5 min to separate the light-green $Ni(OH)_2$ precipitate and supernatant. After decanting the supernatant, the $Ni(OH)_2$ precipitate was mixed with 2 mL of regent grade 1 M KOH and 20 mL of ultra-pure water and then the mixture was re-centrifuged at 8500 rpm for 5 min, which was repeated three times. Afterwards, the precipitate was gently washed with 5 mL of regent grade 1 M KOH which was decanted after washing. The resultant $Ni(OH)_2$ precipitate (Fe adsorbent) was used for purifying the regent grade 1 M KOH.

Electrolyte Purification

In the as-obtained $Ni(OH)_2$-containing centrifuge tube, the $Ni(OH)_2$ precipitate was ultrasonically dispersed in 45 mL of regent grade 1 M KOH, and the suspension was kept for at least 18 h. Finally, the suspension-containing tube was centrifuged at 8500 rpm for 5 min, and the supernatant (Fe-purified 1 M KOH aqueous electrolyte) was decanted and used for electrochemistry.

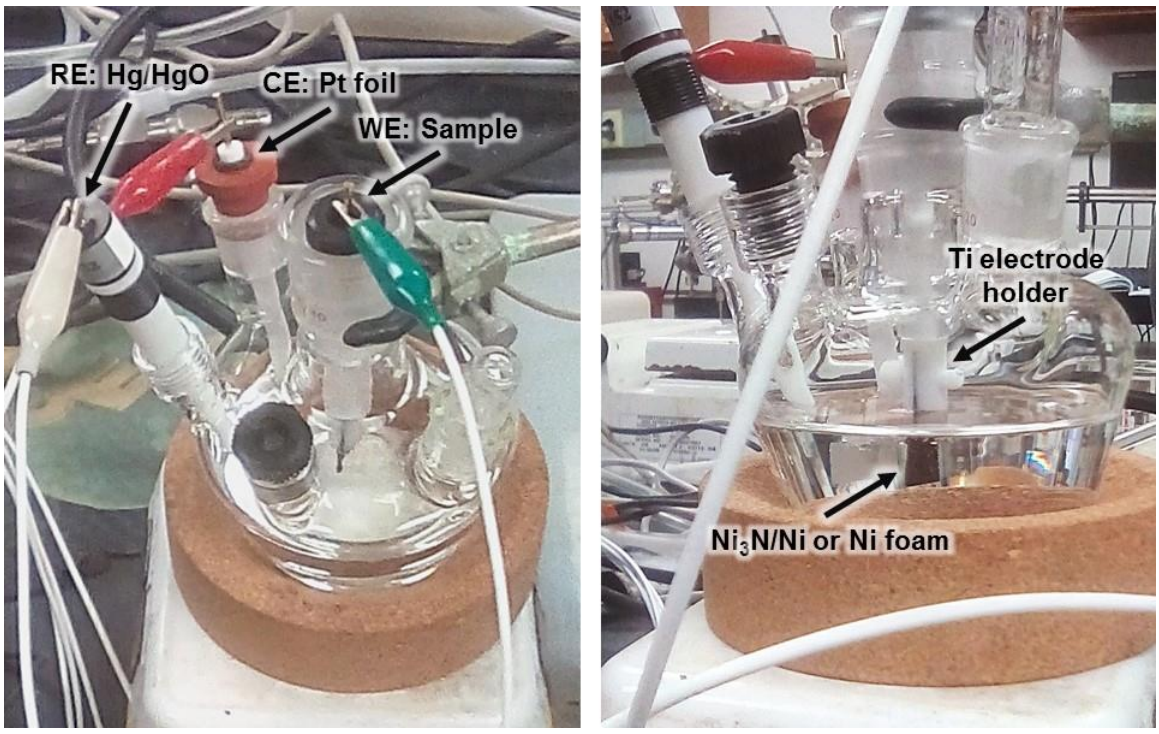

Fig. S1 Digital photographs of a standard three-electrode system including the working electrode (WE), counter electrode (CE), and reference electrode (RE). Prior to the electrochemical tests, the glass flask was washed with dilute aqueous acid solution in order to remove the Fe impurities.

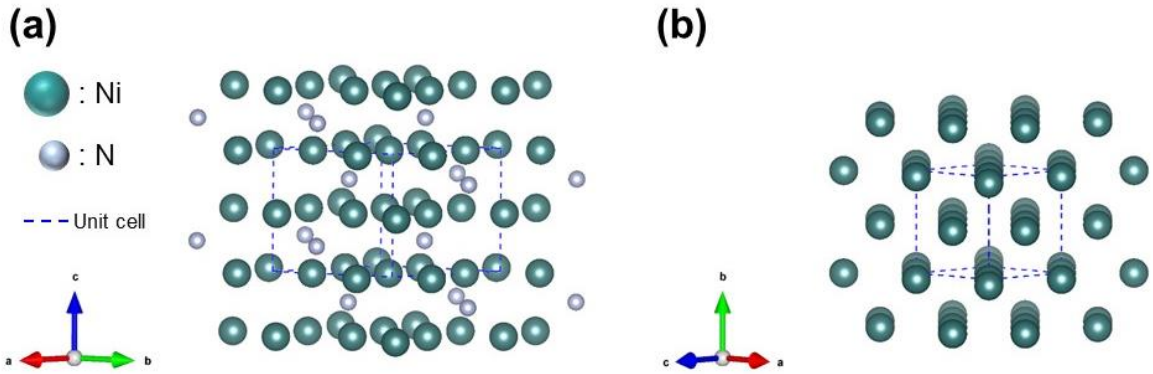

Fig. S2 Schematic illustrations of (a) hexagonal Ni_3N and (b) cubic Ni crystal structures. These crystal structures were drawn with the *VESTA 3* program.[2]

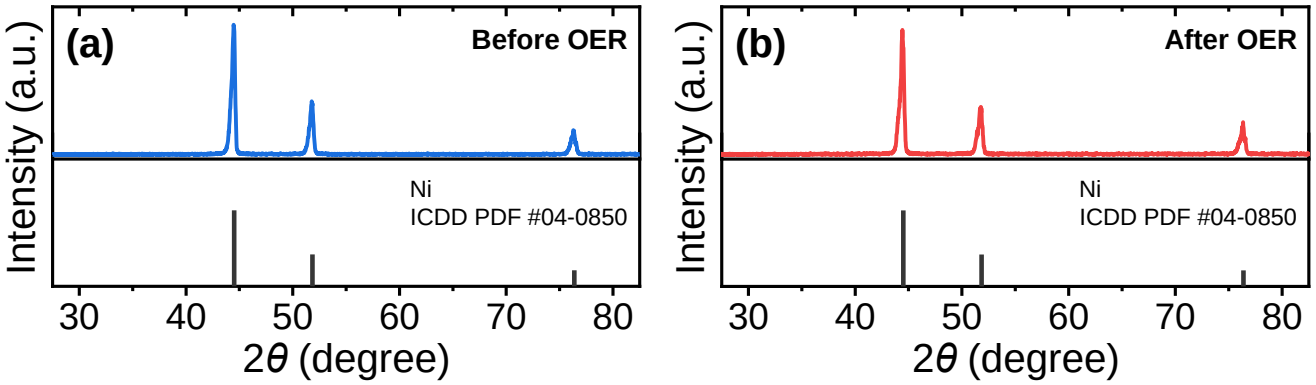

Fig. S3 XRD patterns of Ni foam electrode (a) before and (b) after 1000 cycles of the OER CV (0.25 to 0.75 $V_{Hg/HgO}$) at a scan rate of 50 $mV \cdot s^{-1}$ in purified 1 M KOH aqueous electrolyte.

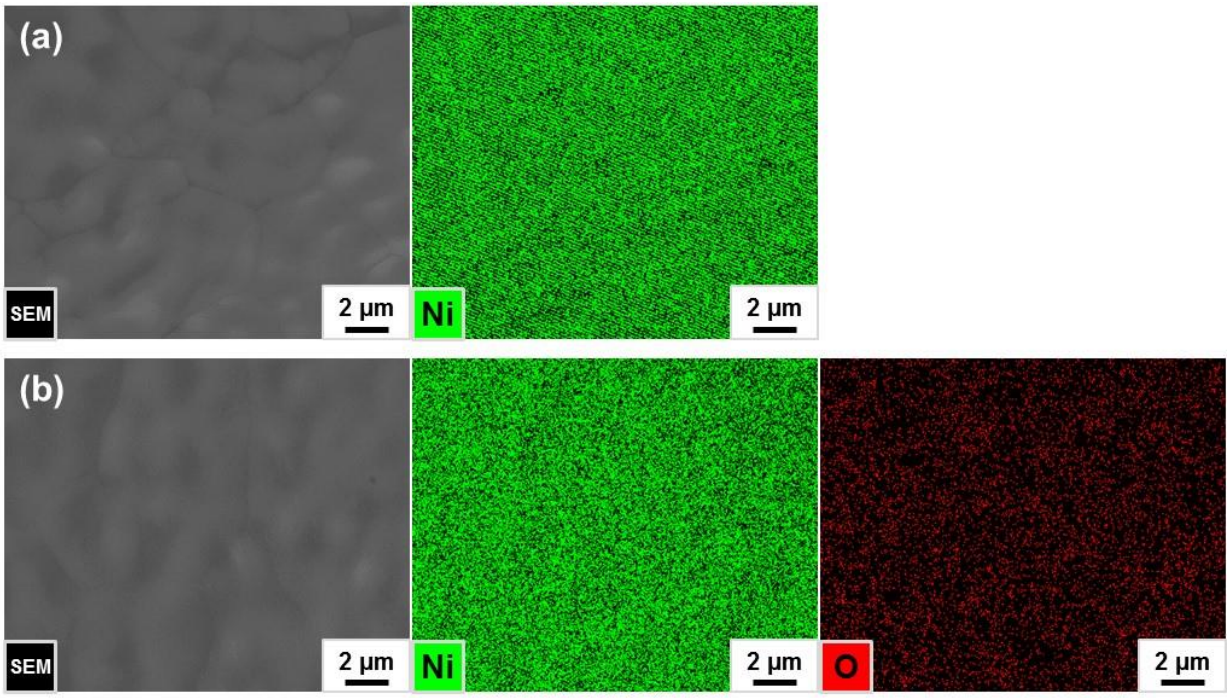

Fig. S4 SEM and EDX elemental mapping images (accelerating voltage: 30 kV) of Ni foam electrode (a) before and (b) after 1000 cycles of the OER CV (0.25 to 0.75 $V_{Hg/HgO}$) at a scan rate of 50 $mV \cdot s^{-1}$ in purified 1 M KOH aqueous electrolyte.

Table S1 SEM-EDX elemental analysis results (atomic percentages and ratios) of pre- and post-OER Ni_3N/Ni and Ni foams corresponding to Figs. 2 and S4

Sample	Ni (at.%)	N (at.%)	O (at.%)	O/Ni at. ratio
Pre-OER Ni_3N/Ni foam	74.780	23.988	1.232	0.016
Post-OER Ni_3N/Ni foam	64.507	20.664	14.829	0.320
Pre-OER Ni foam	100	-	-	-
Post-OER Ni foam	98.763	-	1.237	0.013

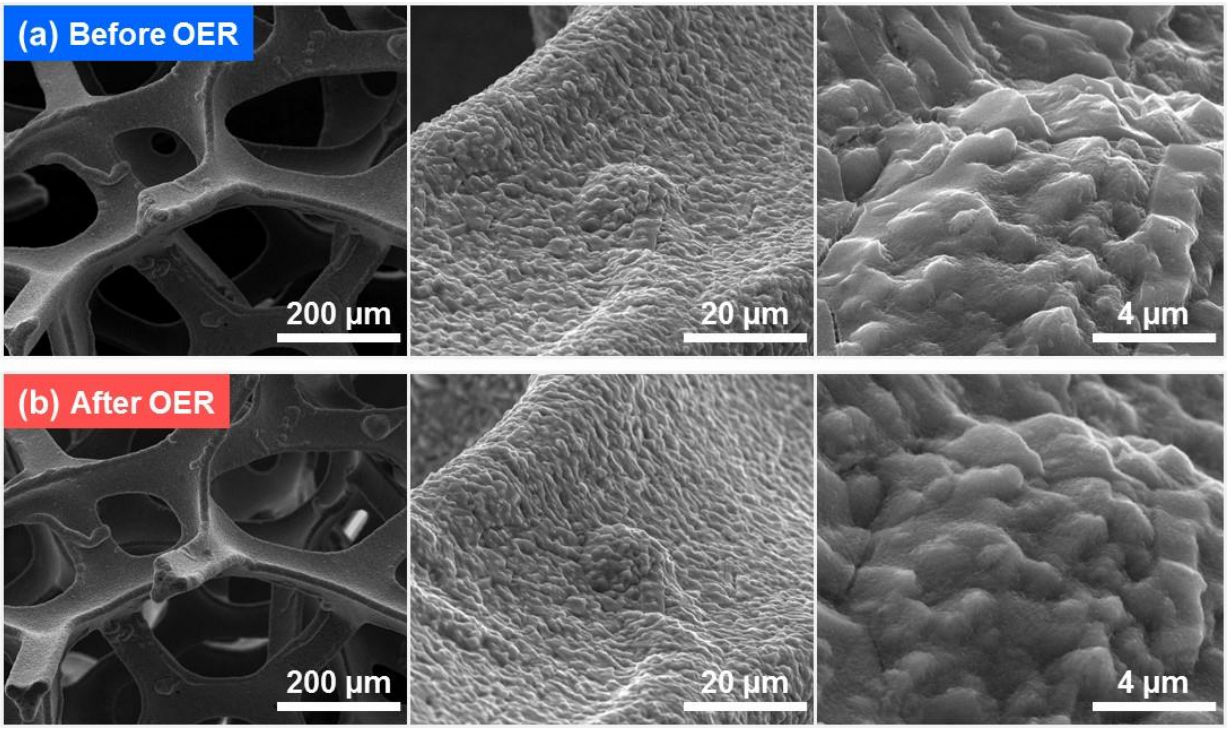

Fig. S5 Low-resolution SEM images of Ni_3N/Ni foam electrode (a) before and (b) after 1000 cycles of the OER CV (0.25 to 0.75 $V_{Hg/HgO}$) at a scan rate of 50 $mV \cdot s^{-1}$ in purified 1 M KOH aqueous electrolyte. Notably, the images were taken at the same position before and after the OER CV test.

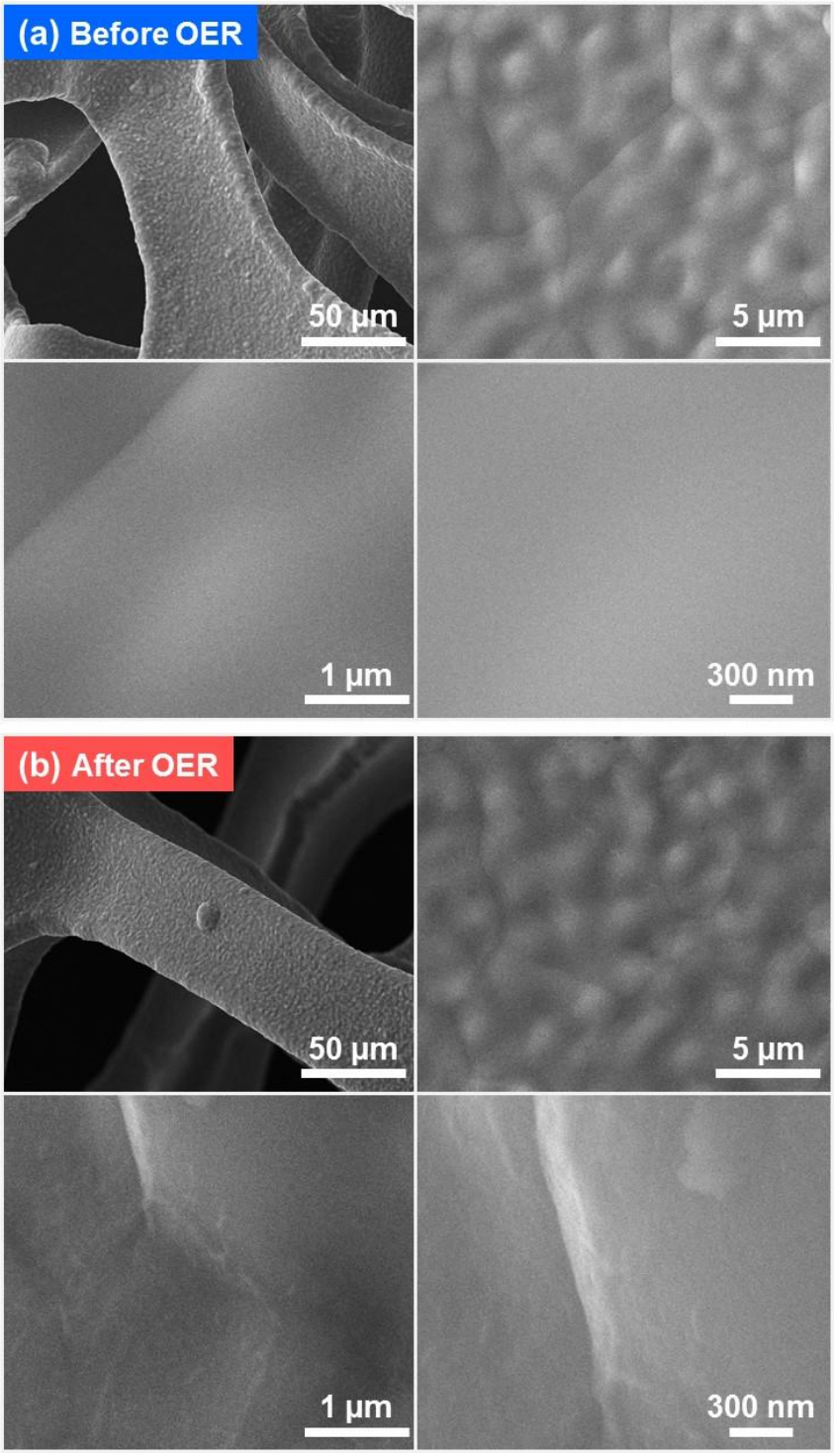

Fig. S6 Low- and high-resolution SEM images of Ni foam electrode (a) before and (b) after 1000 cycles of the OER CV (0.25 to 0.75 $V_{Hg/HgO}$) at a scan rate of 50 $mV \cdot s^{-1}$ in purified 1 M KOH aqueous electrolyte.

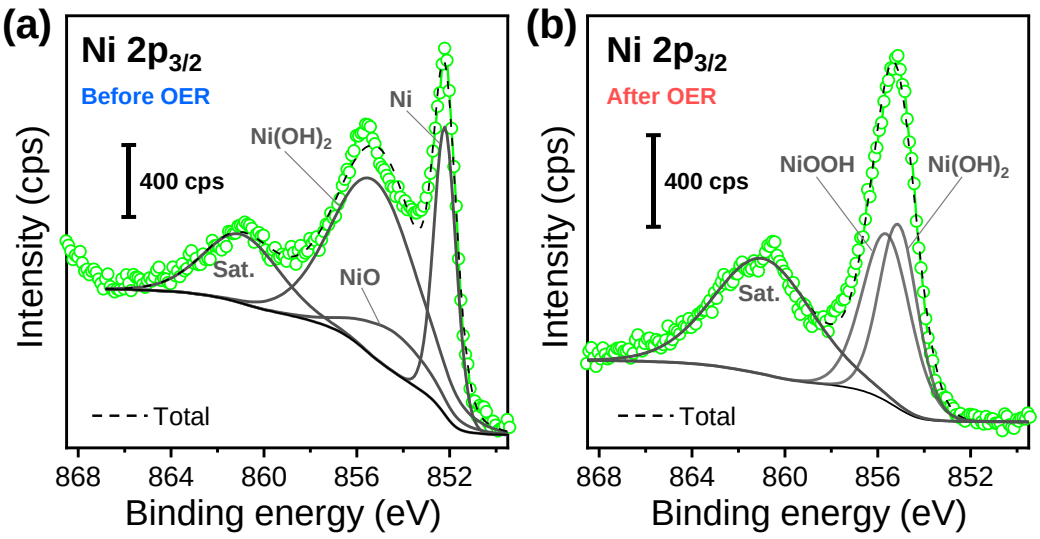

Fig. S7 Ni $2p_{3/2}$ XPS core-level spectra of Ni foam electrode (a) before and (b) after 1000 cycles of the OER CV (0.25 to 0.75 $V_{Hg/HgO}$) at a scan rate of 50 $mV \cdot s^{-1}$ in purified 1 M KOH aqueous electrolyte.

Fig. S7 shows the Ni $2p_{3/2}$ XPS spectra of the pre- and post-OER Ni foams. In the pre- and post-OER Ni $2p_{3/2}$ XPS spectra, the five components can be recognized as (i) metallic Ni (852.2 eV),[3,4] (ii) NiO (854.4 eV),[5] (iii) $Ni(OH)_2$ (around 855.2 eV),[5] (iv) NiOOH (855.6 eV),[5] and (v) satellites (around 860.9 eV),[4] respectively. In the Ni $2p_{3/2}$ spectrum of the pristine Ni foam (Fig. S7a), the signals of oxidized Ni species (*i.e.*, NiO and $Ni(OH)_2$) as well as metallic Ni were confirmed. The presence of the oxidized Ni species is responsible for the partial surface oxidation of Ni due to ethanol- and ultra-pure water-washing and ambient air exposure. After the OER test, the metallic Ni signal completely disappeared and relatively strong signals of $Ni(OH)_2$ and NiOOH appeared. Considering the above XRD, EDX, and XPS results (Figs. S3, S4, and S7), the post-OER Ni foam may possess a Ni@$Ni(OH)_2$/NiOOH core@shell structure.

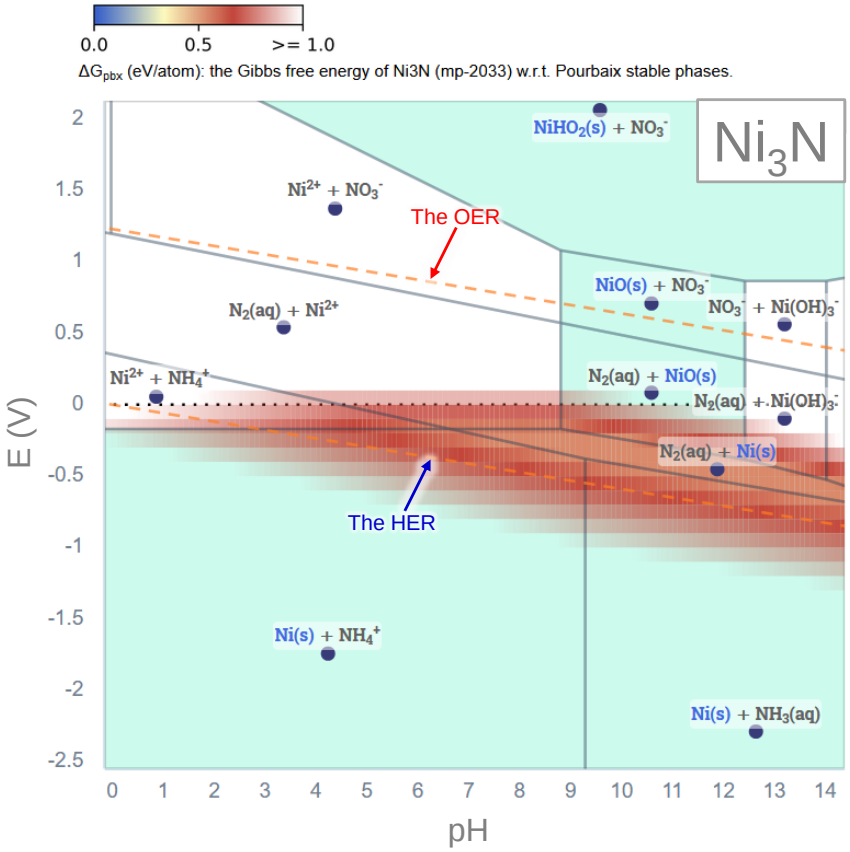

Fig. S8 Electrochemical stability map (Pourbaix diagram and Gibbs free energy overlay) of Ni_3N. The Gibbs free energy overlay indicates areas of aqueous stability for Ni_3N, with blue regions the most stable and red/uncolored regions being least stable. The diagram is produced using the Materials Project (https://materialsproject.org/).[6–8]

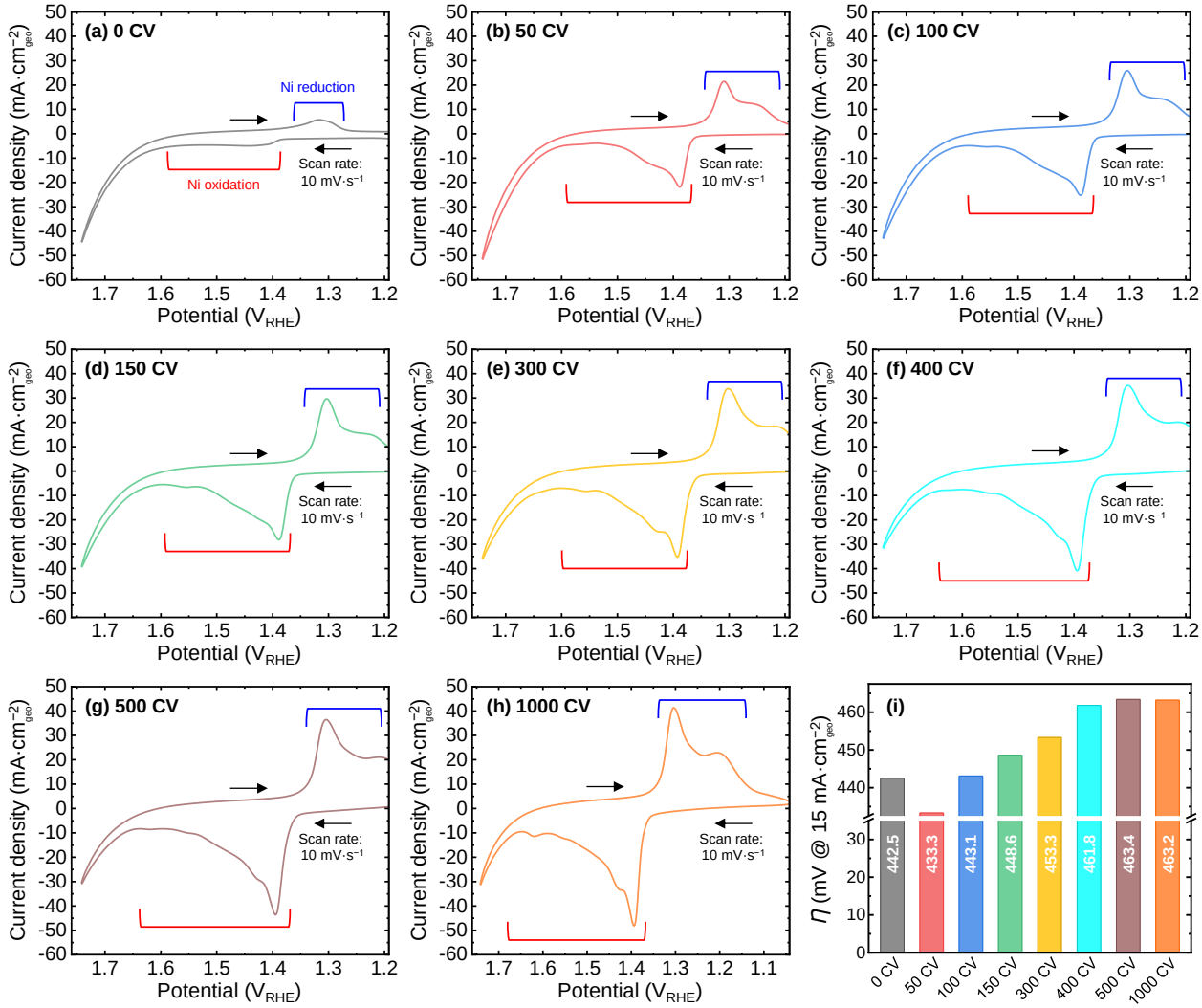

Fig. S9 (a–h) Cyclic voltammograms of Ni_3N/Ni foam electrode after various cycle numbers. (i) OER overpotential (η) transition (based on geometric surface area) for Ni_3N/Ni foam.

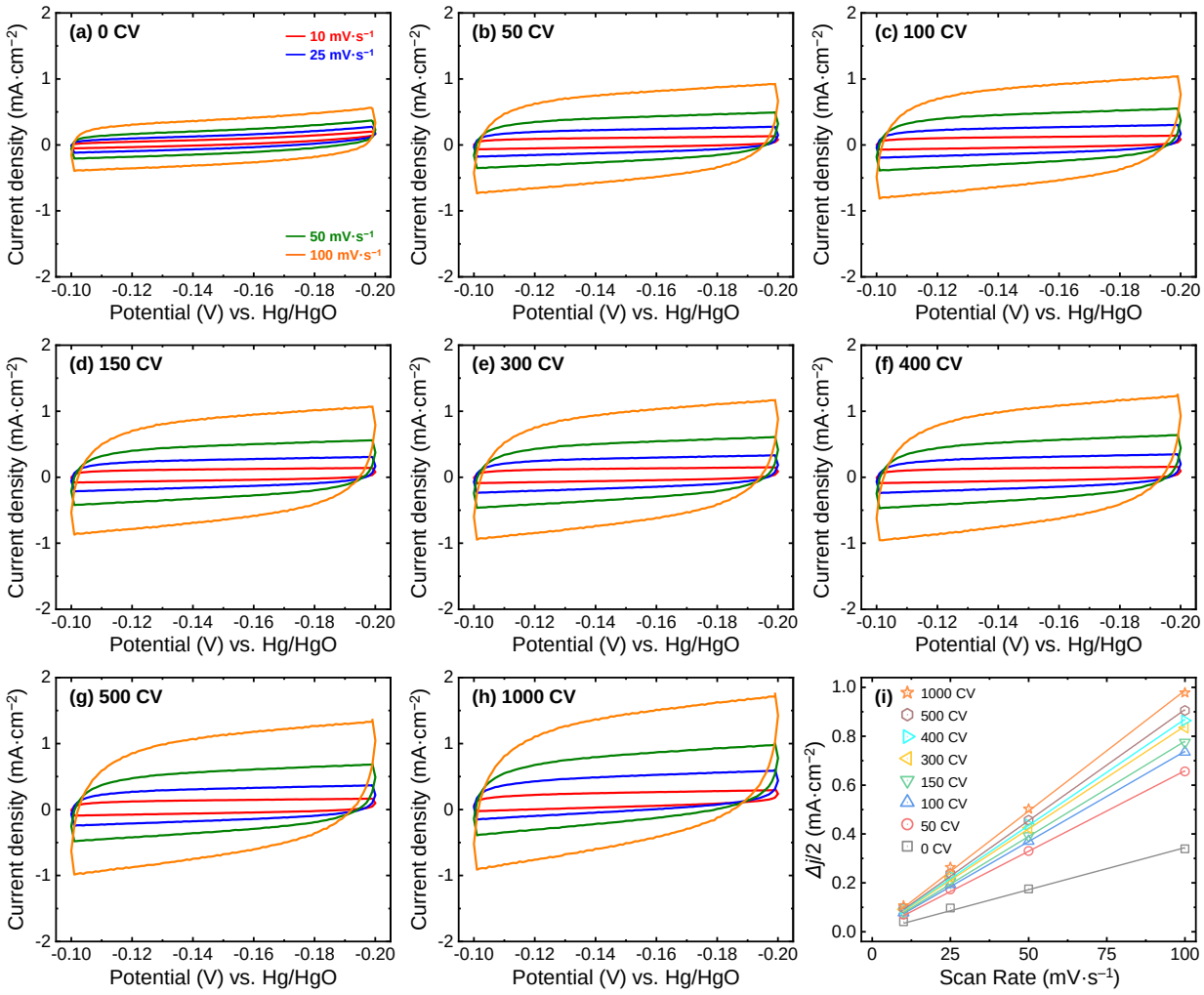

Fig. S10 (a–h) Cyclic voltammetry curves of Ni_3N/Ni foam electrode in the non-faradaic region (−0.2 ~ −0.1 $V_{Hg/HgO}$) at various applied scan rates. (i) Corresponding plots of half the differences between the anodic and cathodic current densities [$\Delta j/2 = (j_a - j_c)/2$] at −0.15 $V_{Hg/HgO}$ *vs*. scan rate of Ni_3N/Ni foam electrode.

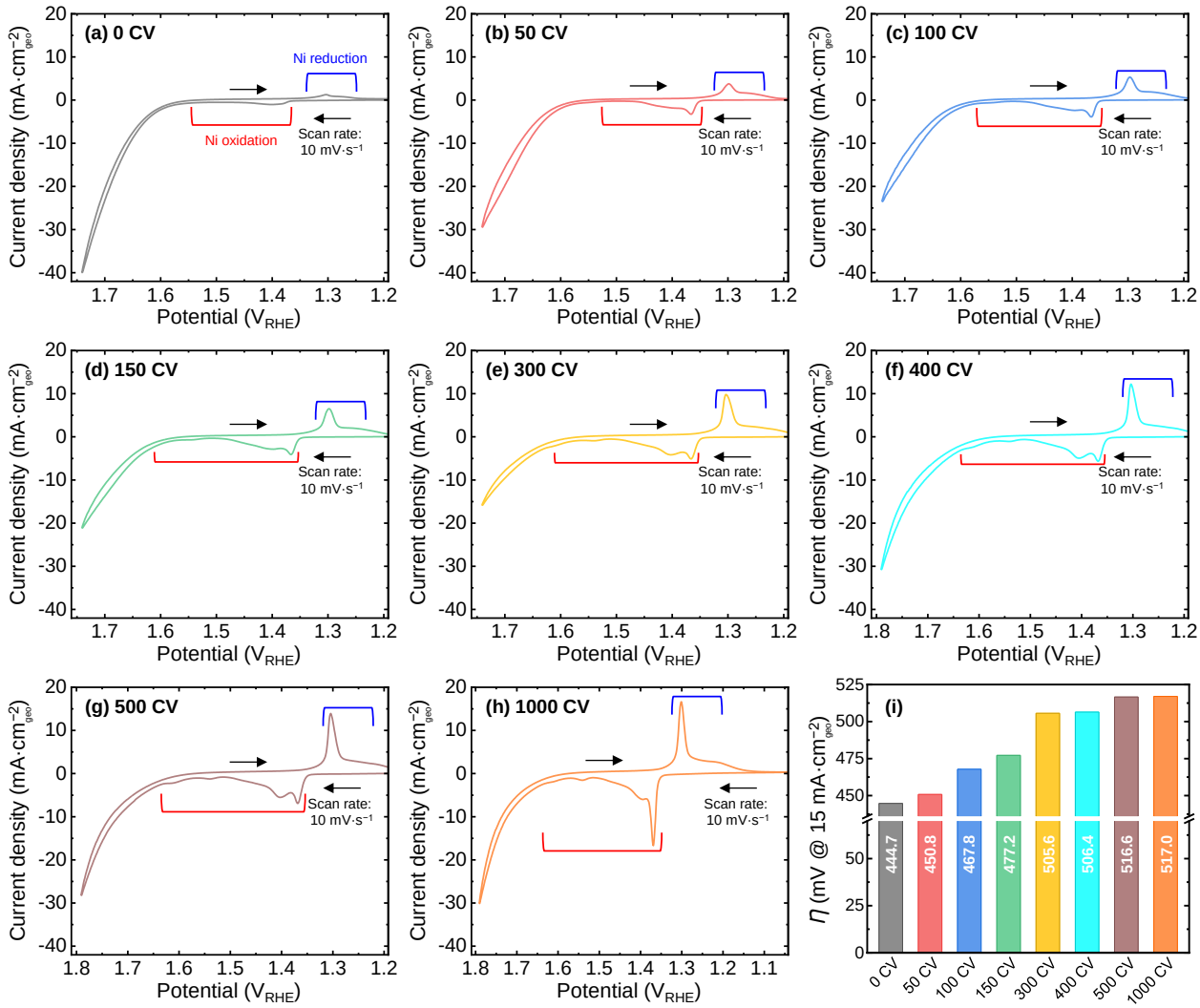

Fig. S11 (a–h) Cyclic voltammograms of Ni foam electrode after various cycle numbers. (i) OER overpotential (η) transition (based on geometric surface area) for Ni foam.

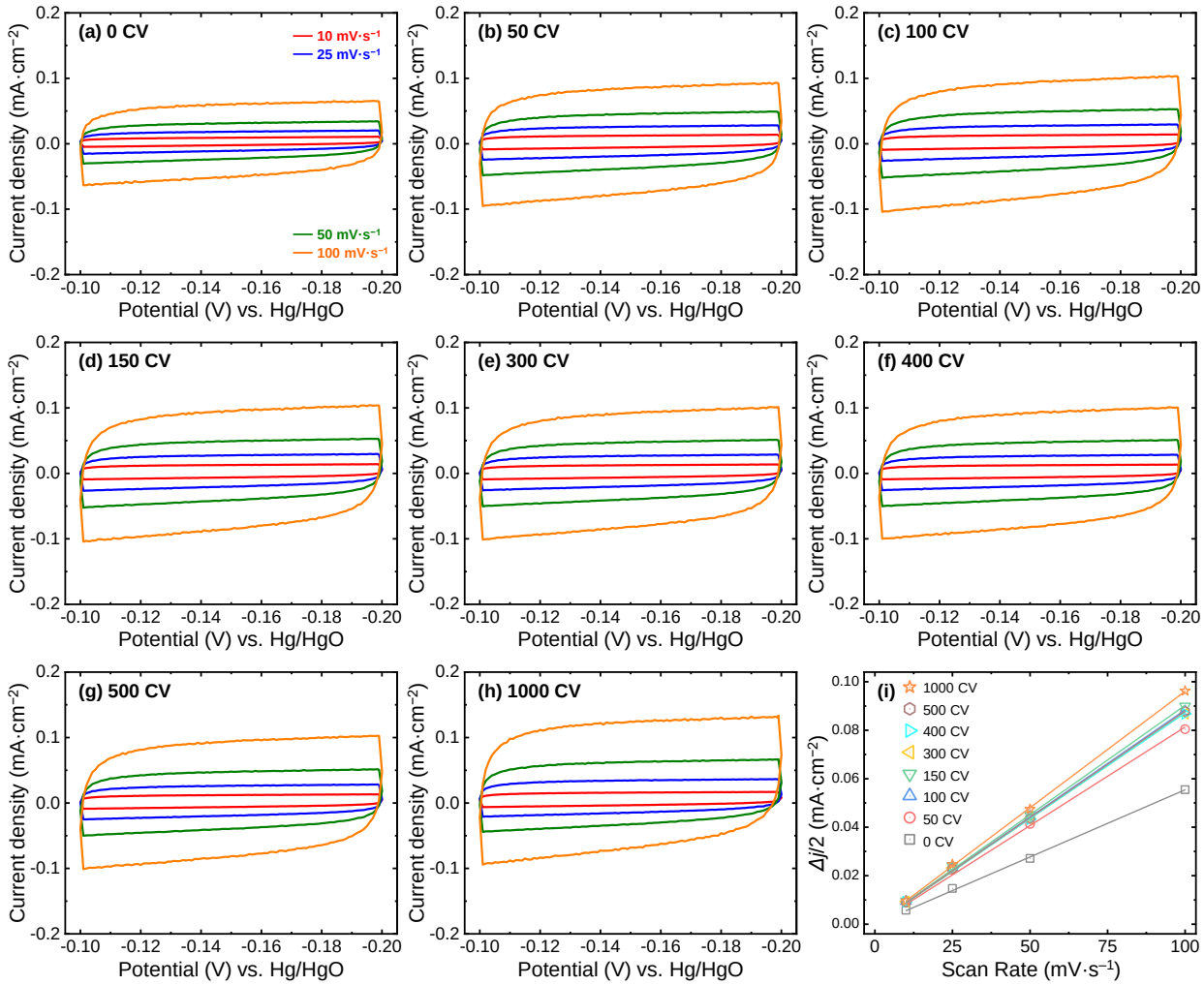

Fig. S12 (a–h) Cyclic voltammetry curves of Ni foam electrode in the non-faradaic region (−0.2 ~ −0.1 $V_{Hg/HgO}$) at various applied scan rates. (i) Corresponding plots of half the differences between the anodic and cathodic current densities [$\Delta j/2 = (j_a - j_c)/2$] at −0.15 $V_{Hg/HgO}$ *vs*. scan rate of Ni foam electrode.

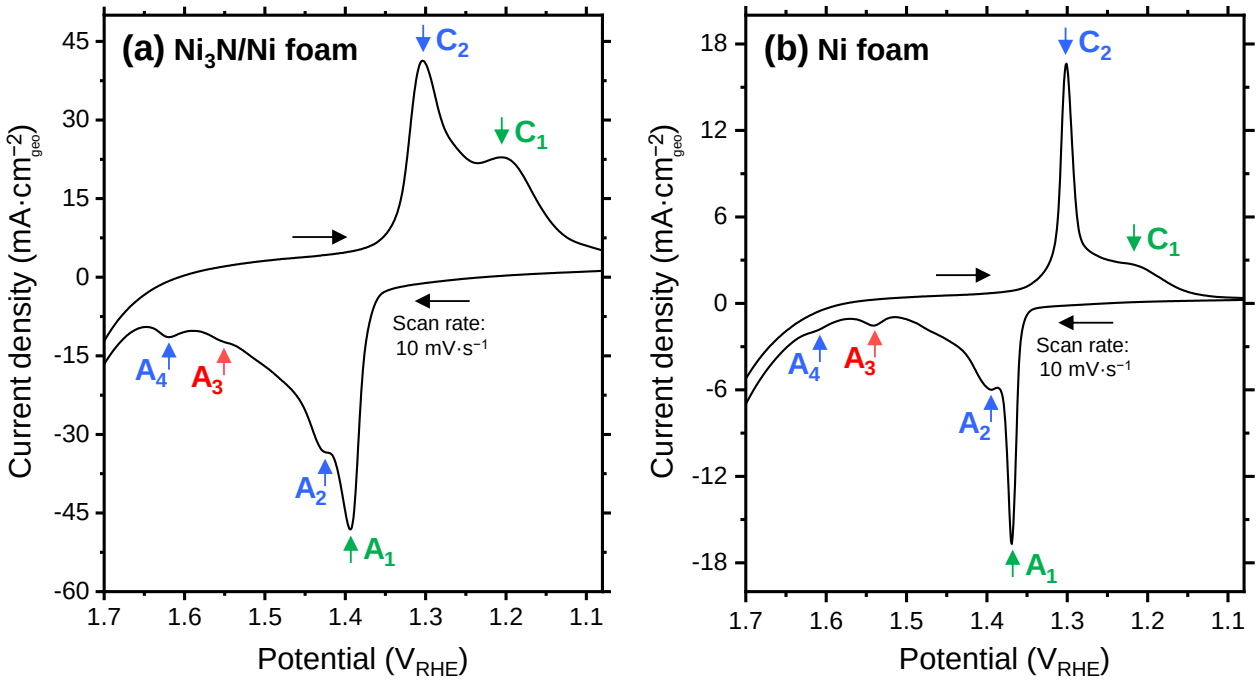

Fig. S13 Magnified cyclic voltammograms of (a) Ni_3N/Ni and (b) Ni foam electrodes after 1000 cycles of the OER CV (0.25 to 0.75 $V_{Hg/HgO}$) at a scan rate of 50 $mV \cdot s^{-1}$ in purified 1 M KOH aqueous electrolyte. The A_1 and A_3 anodic peaks are attributed to γ-NiOOH and Ni^{4+} species (likely NiO_2), respectively.[1] Both the A_2 and A_4 anodic peaks correspond to ordered β-NiOOH.[1] Additionally, The C_1 and C_2 anodic peaks may be assignable to α-$Ni(OH)_2$ and β-$Ni(OH)_2$, respectively.[9,10]

Similar to the report about the $Ni(OH)_2$ film in purified KOH electrolyte,[1] both the Ni_3N/Ni and Ni foam electrodes did not show significant OER currents until > 400 mV overpotential (Fig. S13). Due to the broadened potential windows, the small anodic peaks (the A_4 anodic peaks at around 1.62 V_{RHE} in Fig. S13) were observed. These two phenomena suggest that we could effectively remove the Fe impurities from the KOH electrolyte and the purified electrolyte used here may have the almost same degree of purity as the Fe-free KOH electrolyte prepared by Trotochaud *et al*. Previously, Shalom *et al.* also reported the OER activity of the $Ni_3N/Ni(OH)_2$ electrocatalyst on Ni foam in the Fe-free KOH electrolyte.[11] Contrary to our results, their $Ni_3N/Ni(OH)_2$ electrocatalyst on Ni foam tested in the Fe-free KOH reached a current density of $\sim$ 20 $mA \cdot cm^{-2}_{geo}$ at ~ 400 mV overpotential, and the small anodic

peak at around 1.62 V_{RHE} was visually not observed in the linear sweep voltammogram (LSV). These differences are likely due to the increase in OER activity resulted from the Fe impurities. Since they purified the KOH electrolyte using the procedure reported by Trotochaud *et al.*,[11] the trace Fe was possibly incorporated into their $Ni_3N/Ni(OH)_2$ electrocatalyst on Ni foam from its preparation [likely from the pre-OER CV oxidation (500 cycles) of "Ni/Ni_3N foam" in unpurified 0.1 M KOH].

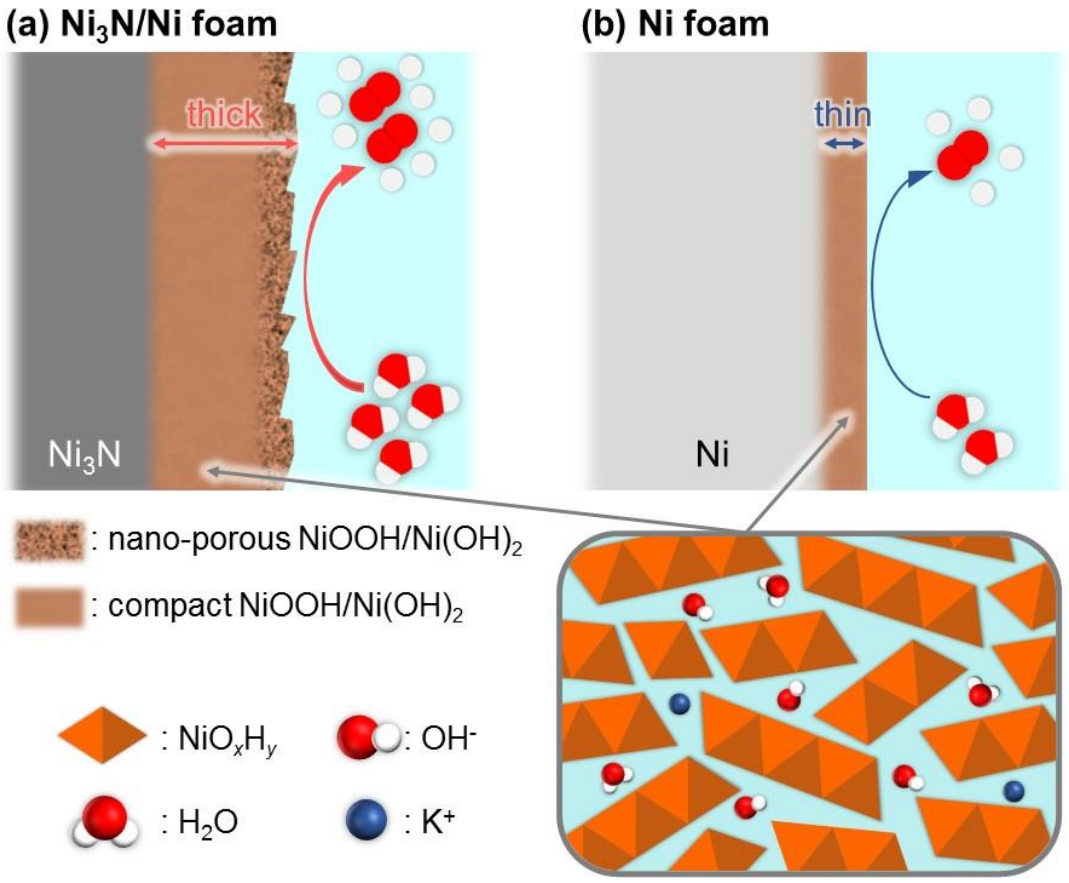

Fig. S14 Schematic illustrations of proposed surface structures of the Ni_3N/Ni and Ni foam electrodes after the OER CV cycling in purified 1 M KOH aqueous electrolyte.

Table S2 A comparison of the Ni_3N and Ni electrocatalysts (after the OER CV and CP tests) in this work with previously reported Ni_3N electrocatalysts (on Ni foams) for the OER

Electrocatalyst	Electrolyte	η (mV)@10 $mA \cdot cm_{geo}^{-2}$	η (mV)@20 $mA \cdot cm_{geo}^{-2}$	C_{dl} ($mF \cdot cm_{geo}^{-2}$)	Refs.
Ni_3N	Purified 1 M KOH	-	482	9.87	This work
Ni		493	534	0.961	
Ni_3N [c]	1 M KOH	262	325	2.12	This work
Ni [c]		435	498	0.158	
Modified Ni/Ni_3N [d]	Purified 1 M KOH	-	~ 403 [a]	-	11
	1 M KOH	-	~ 403 [a]	~ 7.3 [b]	
hNi_3N	1 M KOH	325	~ 363 [a]	5.79	12
Ni_3N	1 M KOH	~ 317 [a]	~ 335 [a]	-	13
Ni_3N	1 M KOH	~ 330 [a]	358	-	14

[a] The values were obtained from the Figures in the previous papers.

[b] The value was calculated using the Figure and the values from the Table in the previous paper.

[c] The samples were tested in the flow cell.

[d] Prior to recording the OER overpotentials, all the sample surfaces were oxidized through 500 CV cycles in unpurified 0.1 M KOH.

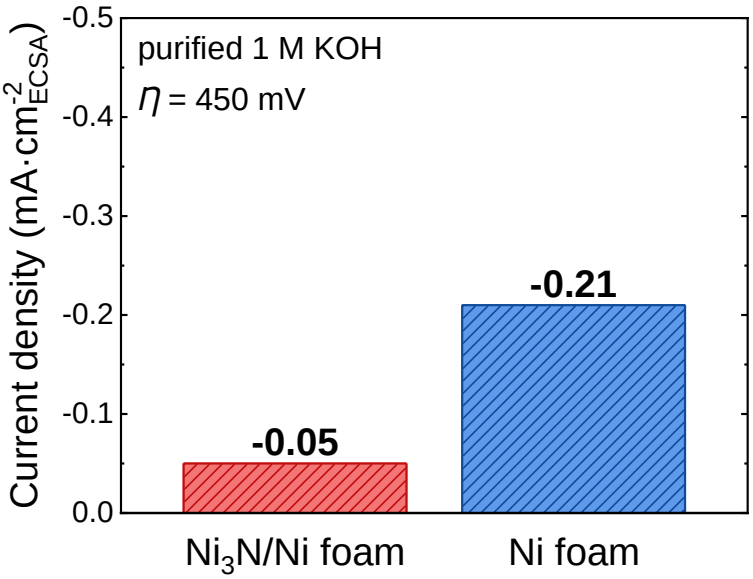

Fig. S15 Specific OER activity (based on ECSA) at η = 450 mV for Ni_3N/Ni and Ni foam electrodes after 1000 cycles of the OER CV (0.25 to 0.75 $V_{Hg/HgO}$) at a scan rate of 50 $mV \cdot s^{-1}$ in purified 1 M KOH aqueous electrolyte. A general specific capacitance of 0.040 $mF \cdot cm^{-2}_{geo}$ was used to calculate the electrochemically active surface areas (ECSAs).[15]

Experimental Details about Flow Cell Tests

Materials

Ni foam (> 99.99%, 80−110 pores per inch) with a thickness of 1.6 mm was purchased from MTI Corporation. Pt gauze (99.9%, 52 mesh) was purchased from Merck KGaA Corporation. Potassium hydroxide (85%, pellets) was purchased from Alfa Aesar. All the aqueous solutions were prepared with deionized water (4.3 $\mu S \cdot cm^{-1}$).

Electrochemical Measurements

Electrochemical water splitting tests were performed during a 20 h period in a 3D-printed electrochemical flow cell.[16] A schematic diagram of the flow cell system is shown in Fig. S16. The as-prepared large Ni foam-based electrode (area: 12 cm^2) was used as a working electrode, while Pt gauze was used as a counter electrode. Three pieces of diamond-shaped turbulence promoter made of ABS polymer were placed between the electrodes, allowing a separation of approximately 2.5 mm. Ni-coated stainless-steel plates were used as current collectors. 500 mL of reagent grade 1 M KOH (pH ~ 14) aqueous electrolyte was recirculated continuously by means of a peristaltic pump (Stenner 85M5). Flow rate was precisely controlled at 6 $L \cdot h^{-1}$ using a calibrated rotameter. Electrolyte was degasified with UHP grade Ar gas for 30 min before any tests.

Electrochemical tests were carried out in a three-electrode configuration using a Ag/AgCl (saturated KCl) reference electrode and an Interface 1000 potentiostat/galvanostat (Gamry). Polarization curves were registered using the LSV technique at a scan rate of 10 $mV \cdot s^{-1}$. Stability tests were performed as chronopotentiometry (CP) runs at a constant value of 10 $mA \cdot cm_{geo}^{-2}$. All the potentials were converted into the reversible hydrogen electrode (RHE) scale [$E_{RHE} = E_{Ag/AgCl} + 0.0591 \times pH + E^{\circ}_{Ag/AgCl}$; $E^{\circ}_{Ag/AgCl}$ (saturated KCl) = 0.199 V at 25 °C]. The electrochemically active surface area (ECSA) was estimated by checking the double-layer capacitance (C_{dl}) through cyclic voltammetry (CV) scans in the non-faradaic region. Before measurement, the open circuit potential (OCP) was registered

for 5 min and then eight CV scans (± 50 mV around the OCP) were recorded with different scan rates: 200 to 10 $mV \cdot s^{-1}$ (*i.e.*, 200, 100, 50, 25, and 10 $mV \cdot s^{-1}$). Cathodic and anodic currents at the center potential were averaged and plotted against the scan rate, giving the linear behavior of an ideal capacitor. The slope of the fitted line was associated with the value of C_{dl}. Finally, to monitor the OER activity and ECSA fluctuation during stability tests, CP was stopped every 4 h and the electrolyte was recirculated for 5 min to dissipate bubbles. Then, LSV and CV scans were registered. In all electrochemical measurements, an 85% *iR* compensation was applied.

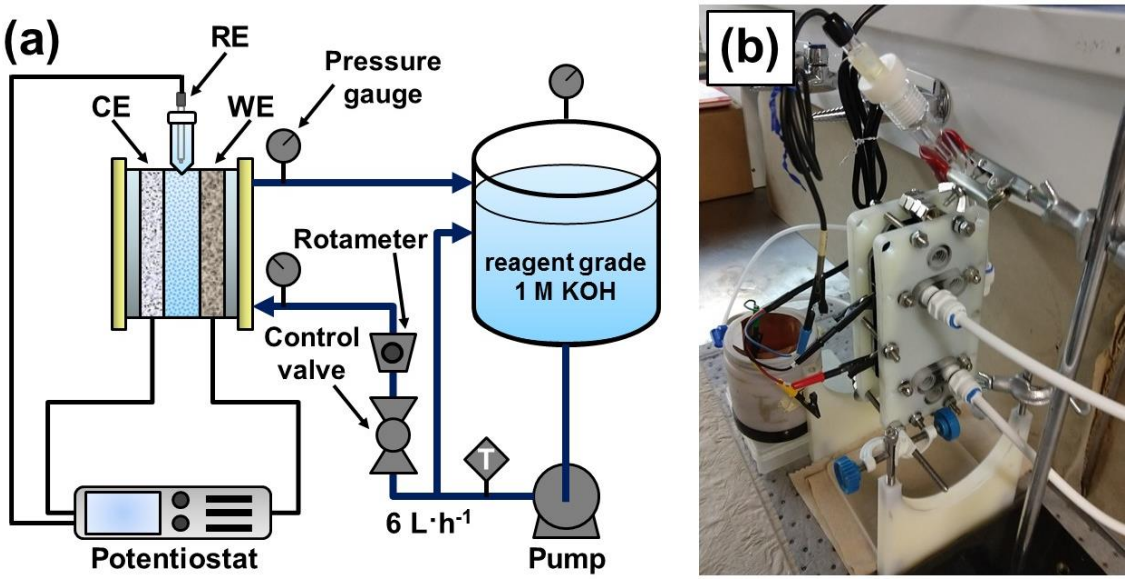

Fig. S16 (a) Schematic illustration and (b) digital photograph of a flow cell system.

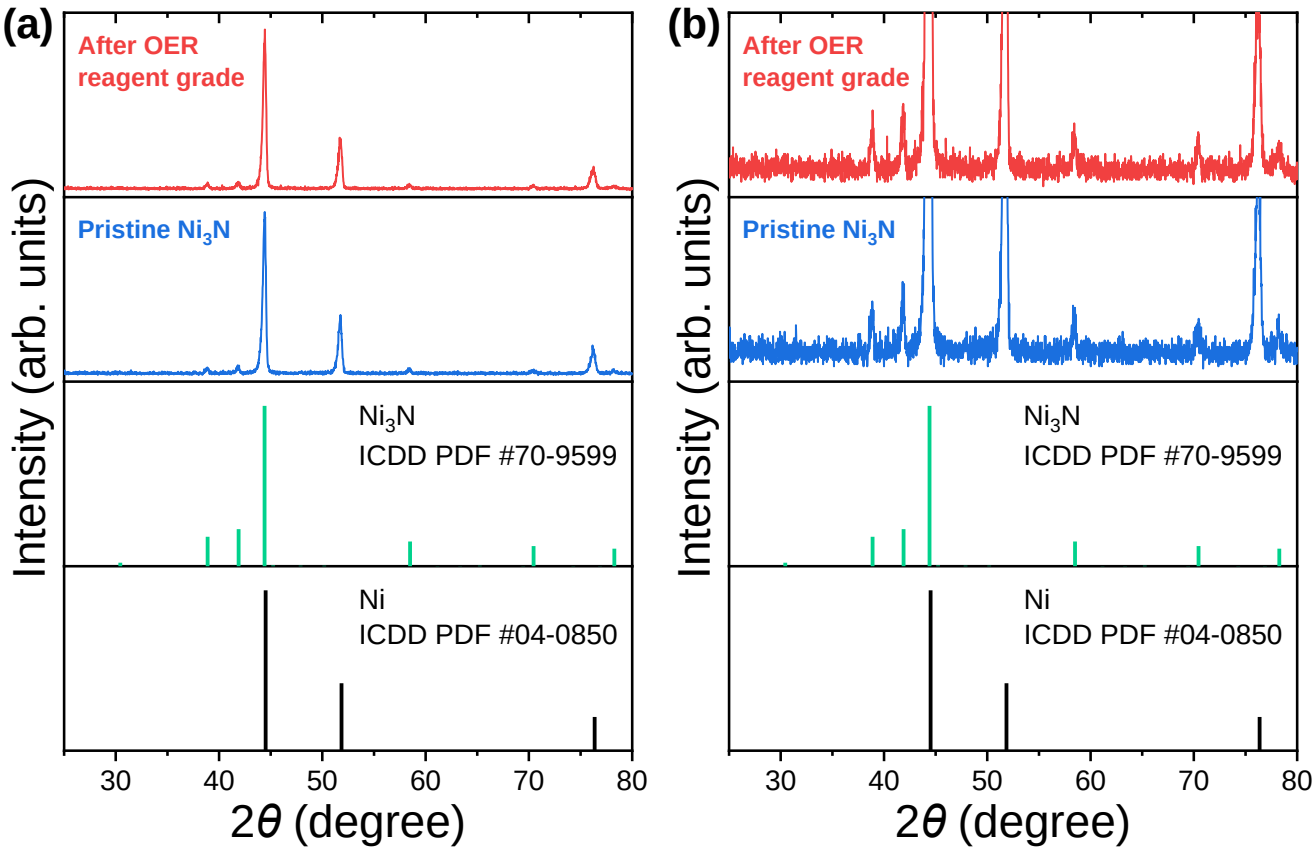

Fig. S17 (a) Unmagnified and (b) magnified XRD patterns of Ni_3N/Ni foam electrode before and after the 20 h OER CP (at 10 $mA \cdot cm_{geo}^{-2}$) in reagent grade 1 M KOH aqueous electrolyte.

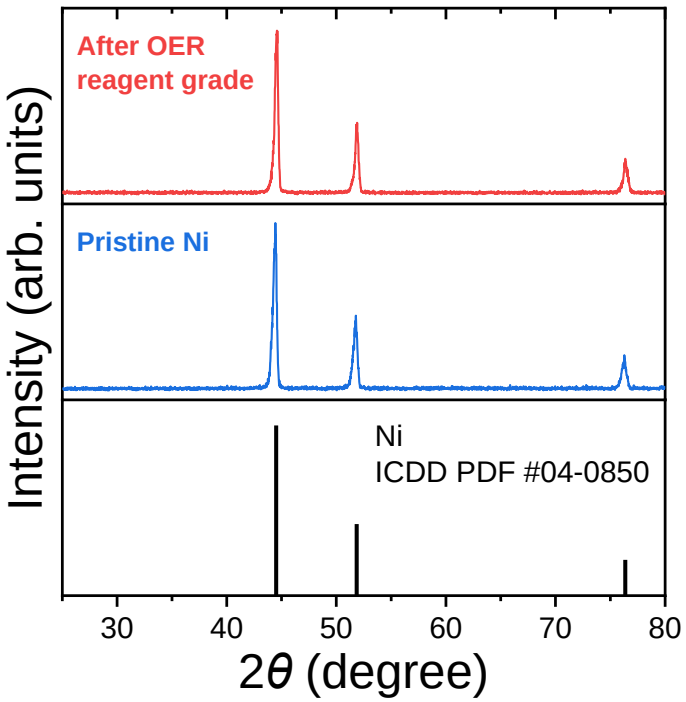

Fig. S18 XRD patterns of Ni foam electrode before and after the 20 h OER CP (at 10 $mA \cdot cm_{geo}^{-2}$) in reagent grade 1 M KOH aqueous electrolyte.

As shown in Figs. S17 and S18, both the Ni_3N/Ni and Ni foams maintained the initial crystal structures after the 20 h OER CP tests. Additionally, the new crystalline phases such as oxides and (oxy)hydroxides were not grown during the long-term CP tests (leaving aside the formation of new amorphous phases).

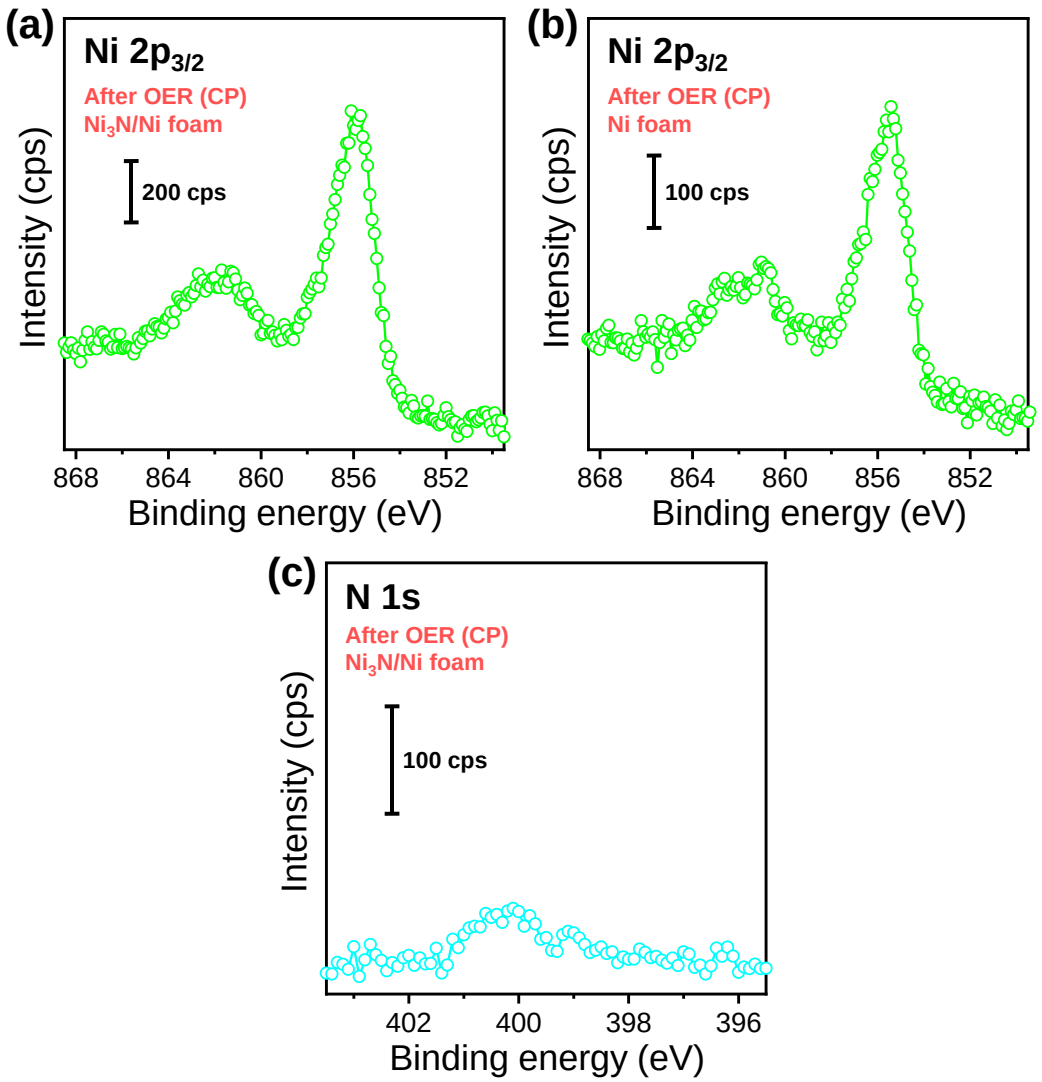

Fig. S19 Ni $2p_{3/2}$ and N 1s XPS core-level spectra of Ni_3N/Ni and Ni foam electrodes after the 20 h OER CP (at 10 $mA \cdot cm_{geo}^{-2}$) in reagent grade 1 M KOH aqueous electrolyte.

Similar to the post-OER CV samples, in the post-OER CP Ni $2p_{3/2}$ spectra (Fig. S19), the peaks corresponding to Ni_3N (852.8 eV)[12,17] and Ni metal (852.2 eV)[3,4] were not confirmed, while the peaks assignable to $Ni(OH)_2$,[5] NiOOH,[5] and sattelites[4] were detected. These post-OER CP XPS results suggest the surface oxidation of Ni_3N and Ni into NiOOH and $Ni(OH)_2$.

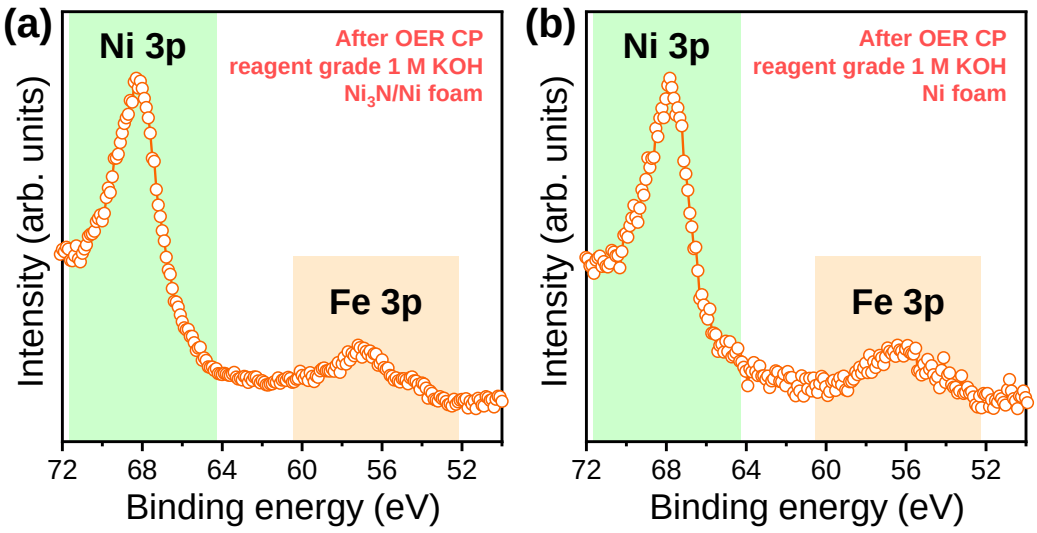

Fig. S20 Ni 3p and Fe 3p XPS core-level spectra of Ni_3N/Ni and Ni foam electrodes after the 20 h OER CP (at 10 $mA \cdot cm_{geo}^{-2}$) in reagent grade 1 M KOH aqueous electrolyte.

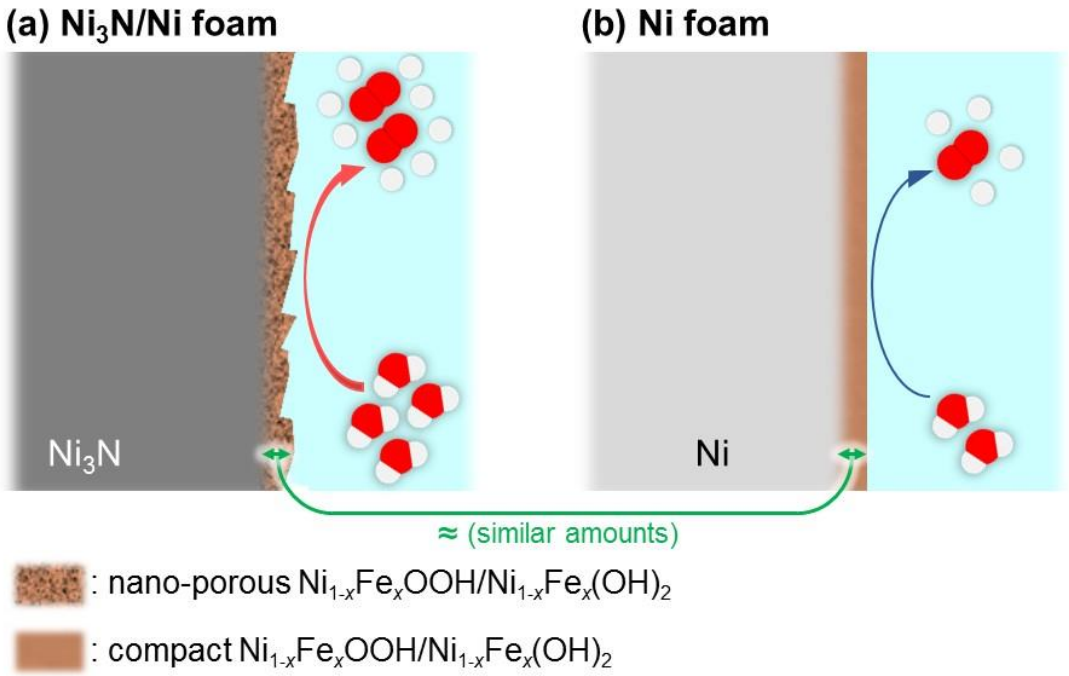

Fig. S21 Schematic illustrations of proposed surface structures of the Ni_3N/Ni and Ni foam electrodes after the OER CP testing in reagent grade 1 M KOH aqueous electrolyte. The post-OER Ni foam surface may have higher Fe incorporation per ECSA than the post-OER Ni_3N foam surface.

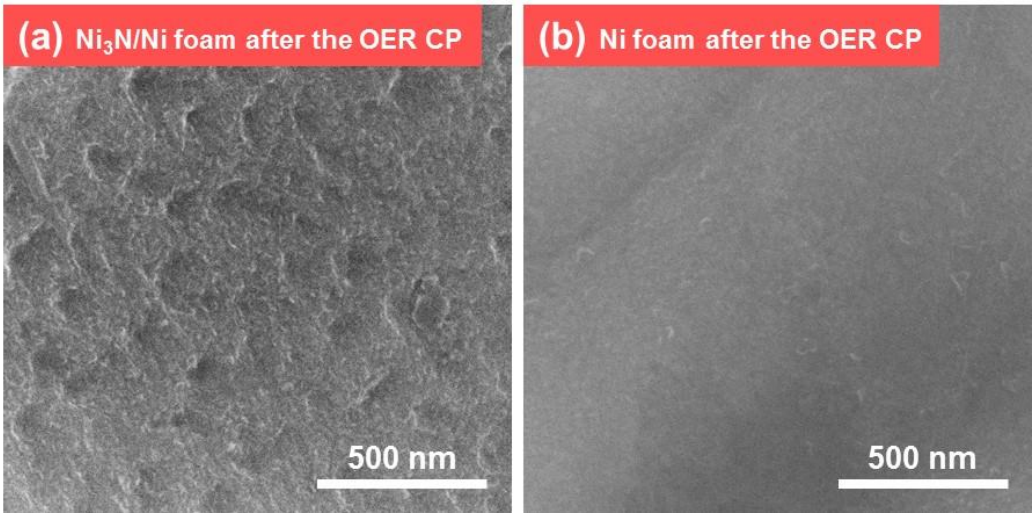

Fig. S22 High-resolution SEM images of (a) Ni_3N/Ni and (b) Ni foam electrodes after the 20 h OER CP (at 10 $mA{\cdot}cm^{-2}_{geo}$) in reagent grade 1 M KOH aqueous electrolyte.

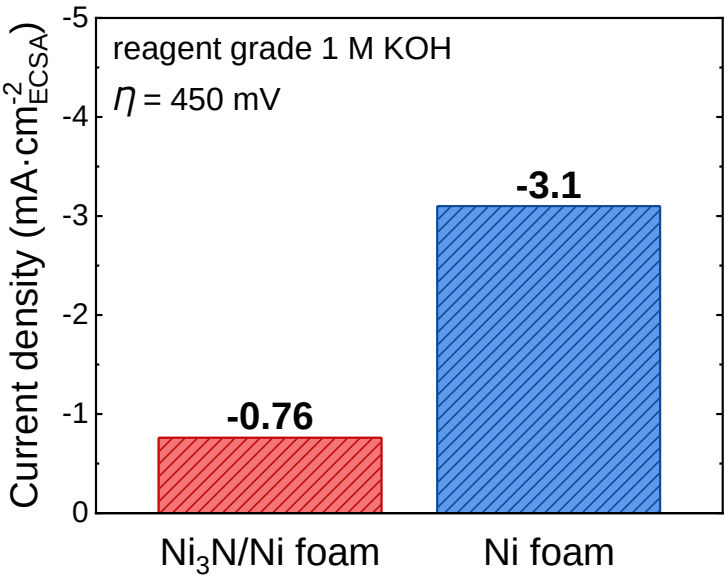

Fig. S23 Specific OER activity (based on ECSA) at η = 450 mV for Ni_3N/Ni and Ni foam electrodes after the 20 h OER CP (at $10\ mA{\cdot}cm_{geo}^{-2}$) in reagent grade 1 M KOH aqueous electrolyte. A general specific capacitance of $0.040\ mF{\cdot}cm_{geo}^{-2}$ was used to calculate the ECSAs.[15]

References

1 L. Trotochaud, S. L. Young, J. K. Ranney and S. W. Boettcher, *J. Am. Chem. Soc.*, 2014, **136**, 6744–6753.

2 K. Momma and F. Izumi, *J. Appl. Crystallogr.*, 2011, **44**, 1272–1276.

3 Z. Bai and B. Zhang, *Nano Mater. Sci.*, 2020, **2**, 151–158.

4 J.-H. Kim, D. H. Youn, K. Kawashima, J. Lin, H. Lim and C. B. Mullins, *Appl. Catal. B: Environ.*, 2018, **225**, 1–7.

5 N. Weidler, J. Schuch, F. Knaus, P. Stenner, S. Hoch, A. Maljusch, R. Schäfer, B. Kaiser and W. Jaegermann, *J. Phys. Chem. C*, 2017, **121**, 6455–6463.

6 K. A. Persson, B. Waldwick, P. Lazic and G. Ceder, *Phys. Rev. B*, 2012, **85**, 235438.

7 A. K. Singh, L. Zhou, A. Shinde, S. K. Suram, J. H. Montoya, D. Winston, J. M. Gregoire and K. A. Persson, *Chem. Mater.*, 2017, **29**, 10159–10167.

8 A. Jain, S. P. Ong, G. Hautier, W. Chen, W. D. Richards, S. Dacek, S. Cholia, D. Gunter, D. Skinner, G. Ceder and K. A. Persson, *APL Mater.*, 2013, **1**, 011002.

9 R. L. Doyle, I. J. Godwin, M. P. Brandon and M. E. G. Lyons, *Phys. Chem. Chem. Phys.*, 2013, **15**, 13737–13783.

10 Y. Mao, B. Zhou and S. Peng, *J. Mater. Sci. Mater. Electron.*, 2020, **31**, 9457–9467.

11 M. Shalom, D. Ressnig, X. Yang, G. Clavel, T. P. Fellinger and M. Antonietti, *J. Mater. Chem. A*, 2015, **3**, 8171–8177.

12 B. Ouyang, Y. Zhang, Z. Zhang, H. J. Fan and R. S. Rawat, *Small*, 2017, **13**, 1604265.

13 M. Jiang, Y. Li, Z. Lu, X. Sun and X. Duan, *Inorg. Chem. Front.*, 2016, **3**, 630–634.

14 X. Liu, X. Lv, P. Wang, Q. Zhang, B. Huang, Z. Wang, Y. Liu, Z. Zheng and Y. Dai, *Electrochim. Acta*, 2020, **333**, 135488.

15 C. C. L. McCrory, S. Jung, I. M. Ferrer, S. M. Chatman, J. C. Peters and T. F. Jaramillo, *J. Am. Chem. Soc.*, 2015, **137**, 4347–4357.

16 R. A. Márquez-Montes, V. H. Collins-Martínez, I. Pérez-Reyes, D. Chávez-Flores, O. A. Graeve and V. H. Ramos-Sánchez, *ACS Sustain. Chem. Eng.*, 2020, **8**, 3896–3905.

17 K. Xu, P. Chen, X. Li, Y. Tong, H. Ding, X. Wu, W. Chu, Z. Peng, C. Wu and Y. Xie, *J. Am. Chem. Soc.*, 2015, **137**, 4119–4125.